Journal of Power Sources 185 (2008) 26–31

Contents lists available at ScienceDirect

Journal of Power Sources

journal homepage: www.elsevier.com/locate/jpowsour

Preparation and electrical properties of yttrium-doped strontium titanate with B-site deficiency

Feng Gao [a], Hailei Zhao [a,b,*], Xue Li [a], Yunfei Cheng [a], Xiong Zhou [a], Fenge Cui [a]

[a] Department of Inorganic Nonmetallic Materials, School of Materials Science and Engineering, University of Science and Technology Beijing, Beijing 100083, China
[b] Beijing Key Lab of New Energy Material and Technology, Beijing 100083, China

ARTICLE INFO

Article history:
Received 6 May 2008
Received in revised form 4 July 2008
Accepted 7 July 2008
Available online 17 July 2008

Keywords:
Solid oxide fuel cell
Anode materials
Yttrium-doped strontium titanate
Nonstoichiometry
Electronic and ionic conductivities

ABSTRACT

Yttrium-doped strontium titanate with B-site deficiency ($Y_{0.08}Sr_{0.92}Ti_{1-x}O_{3-\delta}$) is synthesized via conventional solid-state reaction. The effect of B-site deficiency on the lattice parameter, sinterability, microstructure and electrical properties of $Y_{0.08}Sr_{0.92}TiO_{3-\delta}$ is investigated. The charge compensation mechanism for B-site deficiency is proposed. The limit of B-site deficiency in $Y_{0.08}Sr_{0.92}Ti_{1-x}O_{3-\delta}$ is below 5 mol % in Ar with 5% H_2 at 1500 °C. The sinterability of $Y_{0.08}Sr_{0.92}Ti_{1-x}O_{3-\delta}$ decreases slightly with increasing deficiency level (x). Compared with $Y_{0.08}Sr_{0.92}TiO_{3-\delta}$, the electrical conductivity of $Y_{0.08}Sr_{0.92}Ti_{1-x}O_{3-\delta}$ samples decreases while the ionic conductivity increases with increasing B-site deficient amount. It is assumed that the deficiency of Ti in $Y_{0.08}Sr_{0.92}Ti_{1-x}O_{3-\delta}$ is charge compensated by the increase of oxygen vacancy concentration and the decrease of Ti^{3+} concentration. $Y_{0.08}Sr_{0.92}Ti_{1-x}O_{3-\delta}$ shows a relatively stable electrical conductivity at different oxygen partial pressures and displays an excellent chemical compatibility with YSZ electrolyte below 1200 °C.

1. Introduction

Fuel cells are electrochemical devices that are able to convert chemical energy directly to electrical energy, without any Carnot limitation. They can offer a more efficient and cleaner alternative method of electricity generation than conventional methods [1]. Solid oxide fuel cell (SOFC) is a promising candidate for future energy conversion system because it has higher energy conversion efficiency than other types of fuel cells [2]. It has attracted lots of attentions because of its advantages such as fuel adaptability, simplicity of system design, low emissions and pollution [3,4], and its potential for co-generation of electricity with heat. Solid oxide fuel cell (SOFC) has been considered as one of the solutions for environmental pollution and energy crisis issues. Many efforts are poured into the development of SOFCs for commercialization [5].

Anode is one of the most important components of SOFC, where the fuel is oxidized and electrons are released to the external circuit. In view of its function and working conditions, there are four basic requirements that an anode must meet [6,7]. (1) Good catalytic activity: oxidation of hydrogen and hydrocarbons begins with a chemisorption and dissociation at the surface of the anode. The anode should be catalytically active to minimize polarization loss and promote electro-oxidation. (2) Both ionically and electronically conductive: electrons from the chemical reaction at the anode side must be transported to the external circuit. To complete the charge transfer required for reaction and electricity generation with low ohmic loss, the anode should be both ionically and electronically conductive. (3) Thermal compatibility and chemical stability: since a SOFC is cycled between room temperature and operation temperature, the anode material itself should be thermally and chemically stable in an impurity-containing fuel atmosphere for long-term service, and at the same time it should be also chemically and mechanically compatible with electrolyte and other components in SOFC system. (4) Porosity: to reduce the mass transfer overpotential, a porous structure is necessary for the anode. The gaseous fuel must get contact with the triple-phase boundary (TPB) of the anode or with the surface of the mixed ionic–electronic conductor (MIEC) over as large an area as is feasible. The anode must be fabricated as a porous structure that retains its physical shape over time under operating conditions.

For SOFCs based on yttria-stablized zirconia (YSZ) electrolyte, Nickel/YSZ cermet, which displays excellent catalytic properties for hydrogen oxidation and good current collection, is the most widely used anode material [8–10]. However, since Ni is a good catalyst for hydrocarbon cracking reaction, the use of hydrocarbon

* Corresponding author at: Department of Inorganic Nonmetallic Materials, University of Science and Technology Beijing, Beijing, China. Tel.: +86 10 82376837; fax: +86 10 82376837.
E-mail address: hlzhao@mater.ustb.edu.cn (H. Zhao).

0378-7753/$ – see front matter © 2008 Elsevier B.V. All rights reserved.
doi:10.1016/j.jpowsour.2008.07.015

fuels in a SOFC with Ni-based anode results in carbon deposition and thus irreversible cell degradation [11,12]. This type of anode also suffers from the disadvantage of resistance losses due to the sintering of nickel grain at high operating temperatures, sulfur poisoning and volume instability upon redox cycling. Therefore, the development of new anode materials for SOFCs that operate on hydrocarbons is widely recognized to be an important project.

In recent years, ceramics with both ionic and electronic conductivity at high temperature and in a reducing environment have been received increasing attentions in their applications as SOFC anodes or anode components due to a combination of the following points [13]: (1) reduced interfacial polarization resistance by expanding reaction sites to the whole anode; (2) relatively good compatibility with high-quality electrolytes and mechanical stability during long term service without expansion of metal components; and (3) higher sulfur tolerance compared to metal components. Therefore, considerable efforts have been devoted to developing various mixed ionic and electronic conductor (MIEC) anode materials for the application on fuel-flexible SOFC with sulfur tolerance. The ABO_3 structure of perovskite has been found to be less reactive with H_2S than the Ni-based anode and more resistive to carbon deposition, and show mixed electronic and ionic conduction.

It has been evidenced that materials with perovskite structure are promising candidates for future fuel cell anodes [14,15]. Among of them, strontium titanate ($SrTiO_3$) is highly attractive because of its desirable thermal, chemical stability and semiconducting behavior. Donor-substituted $SrTiO_3$ ceramics show good chemical stability and a relatively high n-type electronic conductivity under reducing conditions. For instance, doping donors such as La^{3+} on the Sr^{2+} site and Nb^{5+} on the Ti^{4+} site convert $SrTiO_3$ into a highly semiconducting n-type material [16,17]. $La_xSr_{1-x}TiO_{3-\delta}$ materials have been reported by Marina et al. [18] to have good dimensional stability upon redox cycling as well as good electronic conductivity in fuel gas atmosphere. Recently, Zhao et al. [19,20] reported the electrical conduction behavior and the chemical compatibility of $Y_xSr_{1-x}TiO_{3-\delta}$ with YSZ, $Y_{0.08}Sr_{0.92}TiO_3$ was found to give the maximum electrical conductivity (71 S cm^{-1}) at 800 °C in pure hydrogen. Hui and Petric [21] measured unusually high electrical conductivity for yttrium-substituted $SrTiO_3$ (SYT) as compared to those with rare-earth substitutes (e.g. La, Pr, Sm, Gd, Yb). The composition $Sr_{0.88}Y_{0.08}TiO_3$ shows a conductivity of 64 S cm^{-1} at 800 °C. All these works mainly focused on the effect of doping elements on the total conductivity of doped $SrTiO_3$ and scarce work concerns the oxygen ionic conductivity. Because the mobility of electrons is usually several orders higher than that of oxygen ions, the electronic conductivity makes an overwhelming contribution to the total conductivity of doped $SrTiO_3$. Hence, the total conductivity practically represents the electronic conductivity of materials. For anode materials of SOFCs, the ionic conductivity is also important as it can extend the TPB area and facilitate the anode reaction, thus decrease the anode polarization. More detailed studies concerning the ionic conductivity of yttrium-doped $SrTiO_3$ are, therefore, desirable.

In this work, deficiency was introduced into the B-site of $Y_{0.08}Sr_{0.92}TiO_{3-\delta}$ to improve the ionic conductivity, where oxygen vacancies are supposed to be produced as charge compensation. The effects of B-site deficiency level on the properties of $Y_{0.08}Sr_{0.92}Ti_{1-x}O_{3-\delta}$ in terms of sinterability and electronic and ionic conductivities as a function of temperature and oxygen partial pressure were investigated. The possible charge compensation mechanism in $Y_{0.08}Sr_{0.92}Ti_{1-x}O_{3-\delta}$ was discussed. The chemical compatibility of $Y_{0.08}Sr_{0.92}Ti_{1-x}O_{3-\delta}$ with YSZ electrolyte was also examined.

2. Experimental

Yttrium-doped strontium titanate with B-site deficiency ($Y_{0.08}Sr_{0.92}Ti_{1-x}O_{3-\delta}$, $x = 0$, 0.01, 0.03, 0.05, 0.07) were prepared by conventional solid-state reaction from Y_2O_3, TiO_2 and $SrCO_3$. After ball-milling for 10 h, the mixture of raw materials was calcined at 1300 °C for 10 h in forming gas (5% hydrogen in argon). The so-obtained powders were ground slightly to destroy agglomerates and then pressed into bars (40 mm-7 mm-3 mm) by uniaxial pressing (ca.115 MPa). The green bars and pellets were sintered in forming gas at 1500 °C for 10 h and then cooled in forming gas with a cooling rate of 3–5 °C min^{-1} in different stages to get dense samples. Sintered bars and pellets were polished for bulk density, microstructure, electrical and ionic conductivity measurements. The synthesis process was monitored by TG-DSC analysis in a NETZSCH STA 409 thermal balance under an atmosphere of flowing air in 200–1300 °C, with a heating rate of 5 °C min^{-1}. The method is based on the weight change and heat flow observed as a function of temperature. The error in the experimental weight gain is estimated to be ±0.05%. The phase identification was achieved by X-ray powder diffraction (XRD) using a Rigaku D/max-A X-ray diffractometer. The densities of all samples were determined by Archimedes' method using water as the liquid medium.

The total electrical conductivity of all samples was measured in forming gas by the standard four-terminal dc method in the temperature range of 50–1000 °C, while the ionic conductivity was determined by electronic blocking electrode method in the temperature range of 500–1000 °C in forming gas. Sintered bars for electrical conductivity measurements were wrapped with four wires which were held in place by small notches cut on the sample surfaces. The setup for ionic conductivity measurement was previously described in detail in literature [22]. All measurements were taken after holding at each temperature to equilibrate for at least 15 min when no significant change in conductivity was observed. Each value of conductivity was the average of four values from different samples. To evaluate the thermal stability of $Y_{0.08}Sr_{0.92}Ti_{1-x}O_{3-\delta}$, the sample was cooled in air after electrical conductivity measurement at 1000 °C in forming gas and then heated up again in forming gas to different temperatures to determine the changes of electrical conductivity. The dependence of conductivities on oxygen partial pressure (P_{O2}) was also investigated under P_{O2} from 10^{-19} to 10^{-14} atm. The oxygen partial pressure was adjusted by changing the temperature of the water vapor saturator. The water vapor partial pressure of the mixture gases was generated by flowing forming gas through the water vapor saturator, which was installed outside the furnace. The temperature of the water vapor saturator was changed from room temperature to 100 °C. Flow rate of these mixture gases was 20 cm^3 min^{-1}. To examine the compatibility of $Y_{0.08}Sr_{0.92}Ti_{1-x}O_{3-\delta}$ with YSZ, the 1300 °C-fired $Y_{0.08}Sr_{0.92}Ti_{1-x}O_{3-\delta}$ powder was mixed with YSZ in the weight ratio of 1:1, followed by uniaxial pressing and sintering at different temperatures. The sintered pellet was crushed and examined by XRD to identify the phases.

3. Results and discussion

The TG–DSC curves of mixture of $SrCO_3$ and TiO_2 are shown in Fig. 1. From 700–1000 °C, the mass curve falls 19.21%, inosculating with the theoretic weight loss of 19.34%, which corresponds to the decomposition of $SrCO_3$ to SrO and CO_2. After that, a sharp exothermic peak appeared at 1013.1 °C, indicating that SrO was reacted with TiO_2 to form $SrTiO_3$. Accordingly, it is concluded that $SrTiO_3$ can be synthesized when the calcining temperature is higher than 1000 °C via conventional solid-state reaction from TiO_2 and $SrCO_3$.

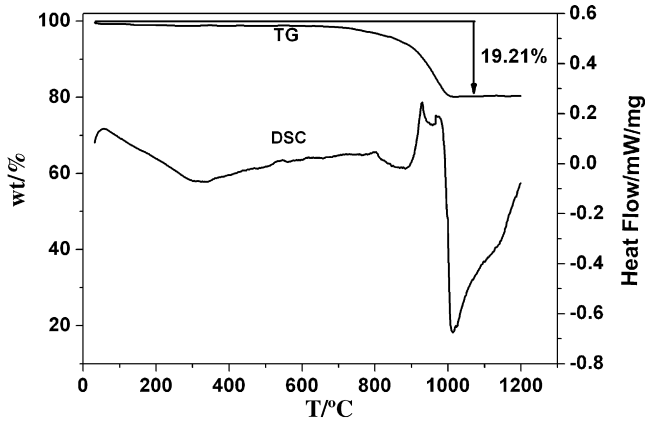

Fig. 1. TG–DSC curves of mixture of $SrCO_3$ and TiO_2.

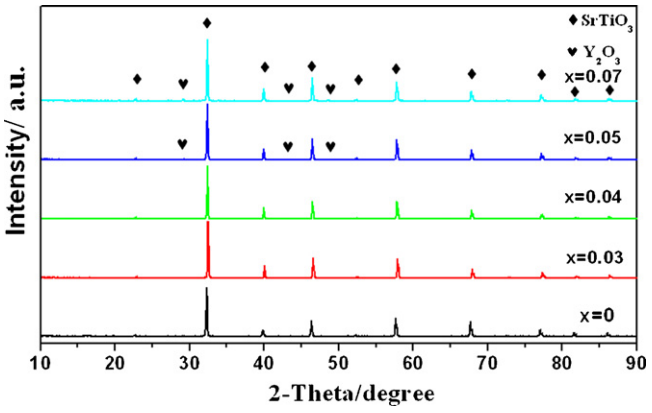

Fig. 2. XRD patterns of $Y_{0.08}Sr_{0.92}Ti_{1-x}O_{3-\delta}$ after sintered at 1500 °C in forming gas.

$Y_{0.08}Sr_{0.92}Ti_{1-x}O_{3-\delta}$ (x = 0, 0.03, 0.04, 0.05, 0.07) powders after being sintered at 1500 °C for 10 h in forming gas were examined by XRD to identify the phases. The results are shown in Fig. 2. Samples with x = 0, 0.03, 0.04 showed a single cubic perovskite structure and no impurity peaks were detected. For samples with x = 0.05 and 0.07, a trace of impurity phase of Y_2O_3 was observed, which can be clearly seen from Fig. 3. Thus, the limit of B-site deficiency in $Y_{0.08}Sr_{0.92}Ti_{1-x}O_{3-\delta}$ at 1500 °C in forming gas is ca. 5 mol%.

Previous studies have showed that doping with yttrium can promote the densification process of $SrTiO_3$ [20]. SEM photographs in Fig. 4 reveal that the samples of $Y_{0.08}Sr_{0.92}Ti_{1-x}O_{3-\delta}$ sintered at 1500 °C for 10 h in forming gas has a highly dense microstructure. However, the density of the samples decreases with increasing deficient level of B-site elements, indicating that B-site deficiency is unfavorable to the densification process of $SrTiO_3$-based materials. Nevertheless, no connecting through pores is observed in these samples.

The bulk density and relative density of $Y_{0.08}Sr_{0.92}Ti_{1-x}O_{3-\delta}$ with different x values are shown in Table 1. The relative densities

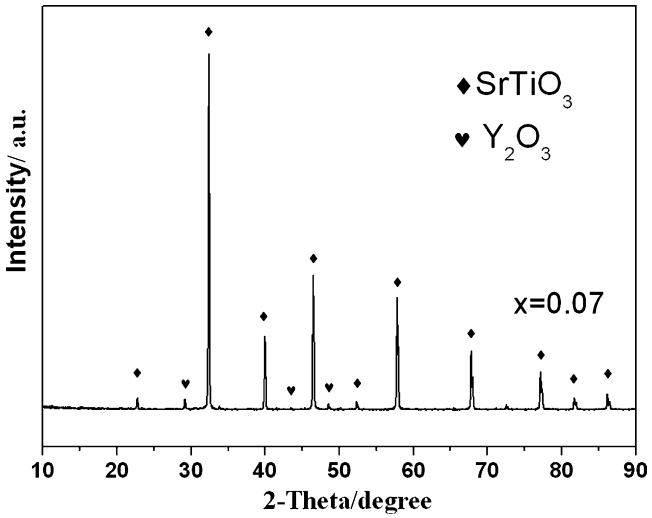

Fig. 3. XRD pattern of $Y_{0.08}Sr_{0.92}Ti_{0.93}O_{3-\delta}$ after sintered at 1500 °C in forming gas.

of samples with x = 0–0.05 are all more than 90% of the theoretical density calculated from the lattice parameters that were obtained by Rietveld refinement. The relative density continuously decreases with increasing x values, suggesting the negative effect of B-site deficiency on the densification process, which is consistent with the result of SEM observation.

The electrical conductivity of $Y_{0.08}Sr_{0.92}Ti_{1-x}O_{3-\delta}$ (x = 0, 0.01, 0.03, 0.05) samples measured in forming gas in the temperature range of 50–1000 °C are shown in Fig. 5. The electrical conductivity is the sum of electronic and ionic conductivities. Due to the low mobility of oxygen vacancies compared to electrons, oxygen vacancies make little contribution to the conductivity of Y-doped $SrTiO_3$. As a result, the total conductivity of $Y_{0.08}Sr_{0.92}Ti_{1-x}O_{3-\delta}$ mostly reflects the electronic conductivity. With increasing temperature, the electrical conductivity increases through a maximum and then decreases. The Arrhenius plot for the temperature dependence of electrical conductivity indicates that there is a linear relationship between $\ln\sigma$ and $1/T$ at low temperature range, suggesting the small polaron hopping conduction mechanism (see Fig. 6). In higher temperature range, however, the electrical conductivity deviates the linear relationship severely and decreases with the temperature, implying the metal-like conduction behavior of $Y_{0.08}Sr_{0.92}Ti_{1-x}O_{3-\delta}$ materials. The electrical conductivities of yttrium-doped strontium titanate with B-site deficiency samples are all lower than the sample with stoichiometric B-site elements, and decreases with the increasing deficient level of B-site elements.

The ionic conductivities of samples $Y_{0.08}Sr_{0.92}Ti_{1-x}O_{3-\delta}$ (x = 0, 0.01, 0.03, 0.05) as a function of temperature are shown in Fig. 7. The ionic conductivities increase with the increasing deficient amount of B-site element, suggesting that the B-site deficiency results in the increase of oxygen vacancy concentration.

Table 1
Theoretical density, bulk density and relative density of $Y_{0.08}Sr_{0.92}Ti_{1-x}O_{3-\delta}$ sintered at 1500 °C for 10 h

Samples	Lattice parameter (Å)	Bulk density (g cm^{-3})	Theoretical density (g cm^{-3})	Relative density (%)
$Y_{0.08}Sr_{0.92}TiO_{3-\delta}$	3.9019	4.6303	5.1297	90.264
$Y_{0.08}Sr_{0.92}Ti_{0.99}O_{3-\delta}$	3.8923	4.8124	5.1667	93.142
$Y_{0.08}Sr_{0.92}Ti_{0.97}O_{3-\delta}$	3.8980	4.7428	5.1452	92.179
$Y_{0.08}Sr_{0.92}Ti_{0.95}O_{3-\delta}$	3.9034	4.6535	5.1237	90.823

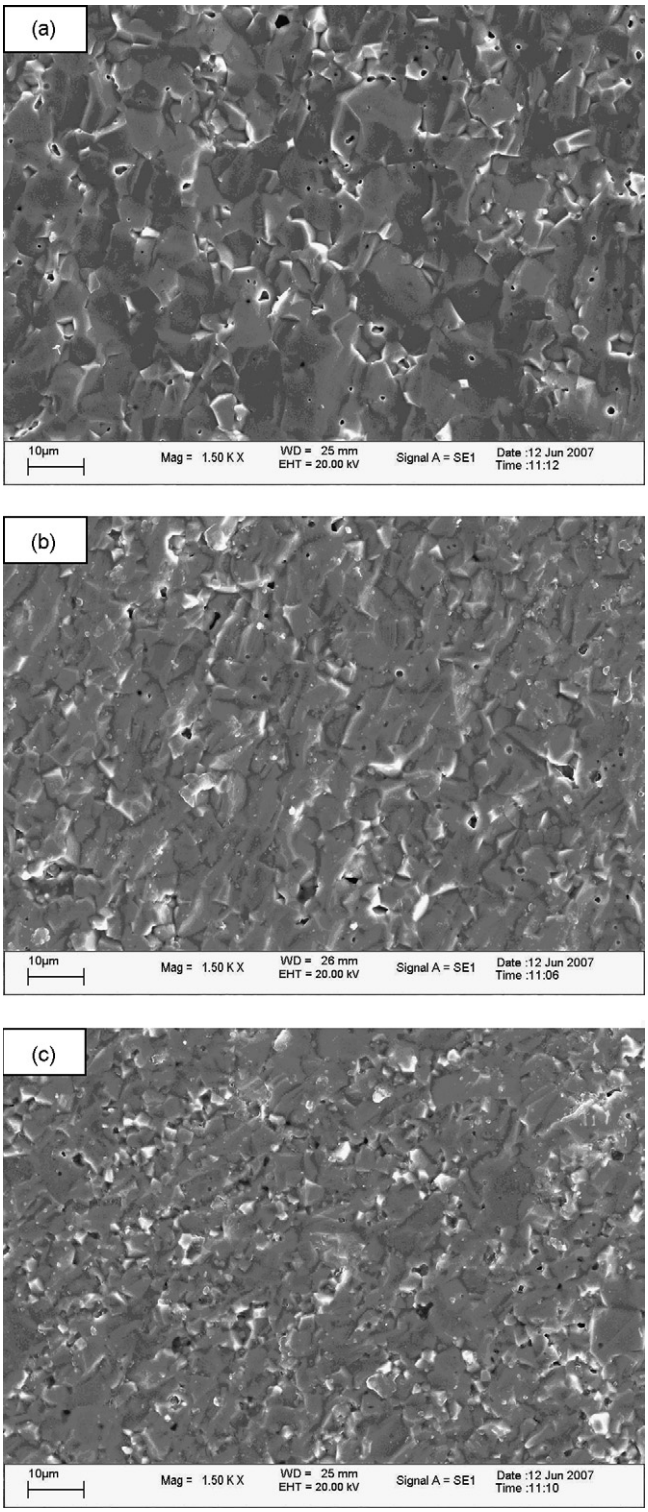

Fig. 4. SEM micrographs of fracture surfaces of $Y_{0.08}Sr_{0.92}Ti_{1-x}O_{3-\delta}$ sintered at 1500 °C for 10 h (a: $x = 0.01$, b: $x = 0.03$, c: $x = 0.05$).

Based on the defect chemistry, the defects caused by Y-doping in $SrTiO_3$ can be expressed as:

$$Y_2O_3 \xrightarrow{SrTiO_3} 2Y_{Sr}^{\bullet} + 2Ti_{Ti}^{\prime\bullet} + 3O_O^{\times} \quad (1)$$

where $Ti_{Ti}^{\prime}$ stands for Ti^{3+} located on Ti^{4+}-site. Under reducing atmosphere, lattice oxygen may loss and thus oxygen vacancies will be

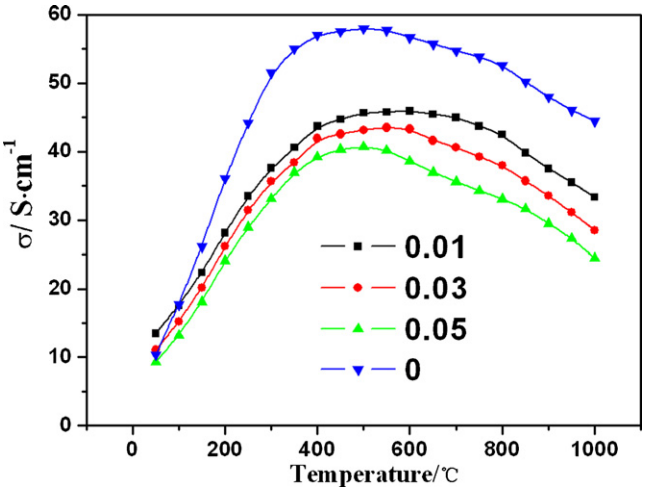

Fig. 5. Temperature dependence of electrical conductivity of $Y_{0.08}Sr_{0.92}Ti_{1-x}O_{3-\delta}$ measured in forming gas at different temperatures.

generated,

$$2TiO_2 \rightarrow 2Ti_{Ti}^{\prime} + 3O_O^{\times} + V_O^{\bullet\bullet} + \frac{1}{2}O_2(g) \quad (2)$$

The concentration of Ti^{3+} with a localized electron, therefore, depends on the doping concentration of Y and the oxygen vacancy concentration. There is

$$[Ti_{Ti}^{\prime}] = [Y_{Sr}^{\bullet}] + 2[V_O^{\bullet\bullet}] \quad (3)$$

For 0.08 mol Y doped $SrTiO_3$ with oxygen vacancy content of δ, there is $[Ti^{3+}] = 0.08 + 2\delta$. The solid solution formula can be described as $Sr_{0.92}Y_{0.08}Ti_{0.08+2\delta}^{3+}Ti_{1-(0.08+2\delta)}^{4+}O_{3-\delta}$. Y-doping on A-site as a donor element can increase the concentration of Ti^{3+} as charge compensation and thus increase the electronic conductivity [20]. For 0.08 mol Y doped $SrTiO_3$ with B-site deficiency, the chemical formula is $Y_{0.08}Sr_{0.92}Ti_{1-x}O_{3-\delta}$. Ti-deficiency will cause the generation of oxygen vacancy and/or the decrease of Ti^{3+} concentration as charge compensation. The corresponding defect reactions can be written as Eqs. (4) and (5),

$$Ti_{Ti}^{\times} + 2O_O^{\times} \rightarrow V_{Ti}^{\prime\prime\prime\prime\prime} + 2V_O^{\bullet\bullet} + TiO_2 \quad (4)$$

$$4Ti_{Ti}^{\prime} + O_2(g) \rightarrow V_{Ti}^{\prime\prime\prime\prime\prime} + 3Ti_{Ti}^{\times} + TiO_2 \quad (5)$$

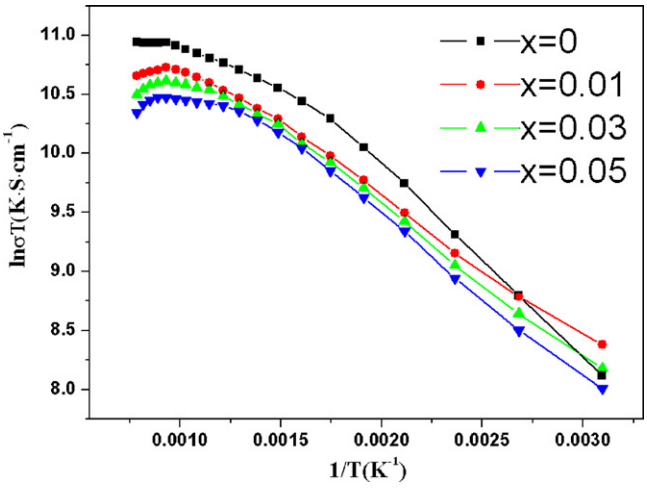

Fig. 6. Temperature dependence of total conductivity of $Y_{0.08}Sr_{0.92}Ti_{1-x}O_{3-\delta}$ measured in forming gas at different temperatures. The solid lines correspond to the Arrhenius model.

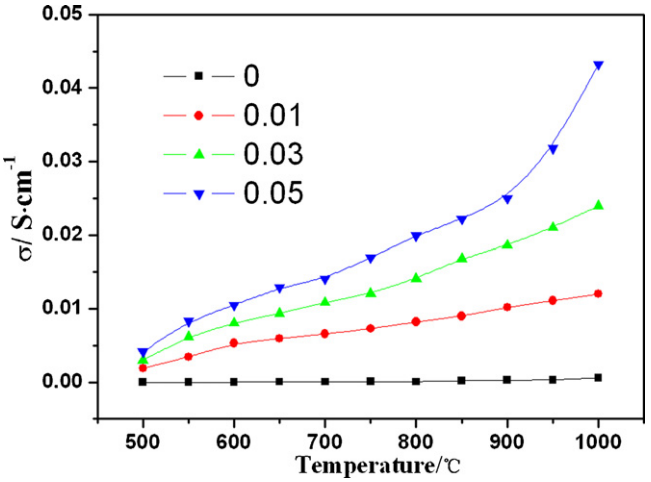

Fig. 7. Temperature dependence of ionic conductivity of $Y_{0.08}Sr_{0.92}Ti_{1-x}O_{3-\delta}$ measured in forming gas at different temperatures.

Considering the electro-neutrality, there is

$$4[V_{Ti}''''] = 2[V_O^{\bullet\bullet}] + [\mathrm{Dec.}(Ti_{Ti}')] \quad (6)$$

where $[\mathrm{Dec.}(Ti_{Ti}')]$ is the decreased Ti_{Ti}' part caused by the deficiency of Ti-ions. The decrease of Ti^{3+} concentration thus results in the increase of average valence of Ti-ions.

If the deficiency of Ti-ion can be compensated completely by the increase of oxygen vacancies, as shown in Eq. (4), the concentration of Ti^{3+} may not change. This will lead to the increasing ionic conductivity and unchanged electronic conductivity. This is not consistent with the experimental results (Figs. 5 and 7). The increase of ionic conductivity of Y-doped $SrTiO_3$ with B-site deficiency indicates the increased oxygen vacancy concentration; whereas the decrease of total electrical conductivity suggests that the excessive negative charge caused by B-site deficiency can not be compensated completely by the generation of oxygen vacancies (Fig. 5). Part of it is compensated by the decrease of Ti^{3+} concentration (Eq. (5)), as a consequence, the electronic conductivity decreases, leading to the decrease of total electrical conductivity.

In SOFC systems, anode is the channel of fuel with a reducing atmosphere and also the place for reaction with a faint oxidizing atmosphere. Therefore, it is necessary for anode material to have stable performance in wide oxygen partial pressure range. As shown in Fig. 8, with the decreasing oxygen partial pressure the electrical conductivity of $Y_{0.08}Sr_{0.92}Ti_{0.97}O_{3-\delta}$ keeps unchanged in the oxygen partial pressure range of 10^{-14}–10^{-17} atm, while shows a slight increase when the oxygen partial pressure is lower than 10^{-17} atm. This indicates the relatively stable electrical conductivity and good structural stability of $Y_{0.08}Sr_{0.92}Ti_{1-x}O_{3-\delta}$ under different reducing conditions. The slight increase in conductivity with decreasing oxygen pressure comes from the release of lattice oxygen into the surrounding atmosphere, which will result in the increase of both oxygen vacancies and electrons, as shown in Eq. (7)

$$O_O^{\times} \rightarrow V_O^{\bullet\bullet} + 2e' + \tfrac{1}{2}O_2(g). \quad (7)$$

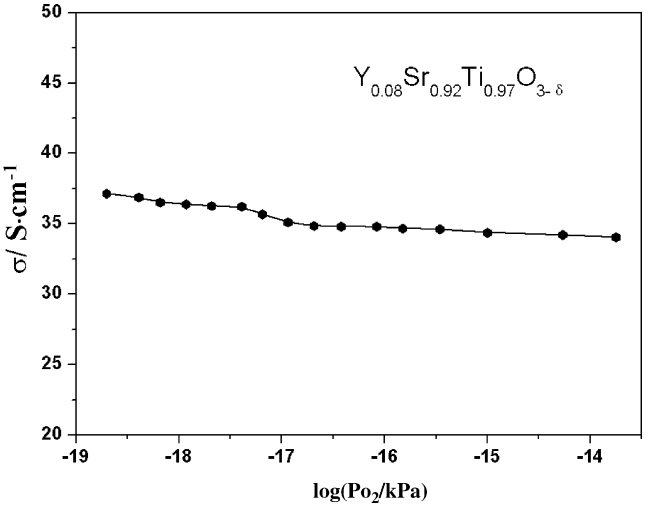

Fig. 8. Effect of oxygen partial pressure (P_{O_2}) on electrical conductivity of $Y_{0.08}Sr_{0.92}Ti_{0.97}O_{3-\delta}$ at 800 °C.

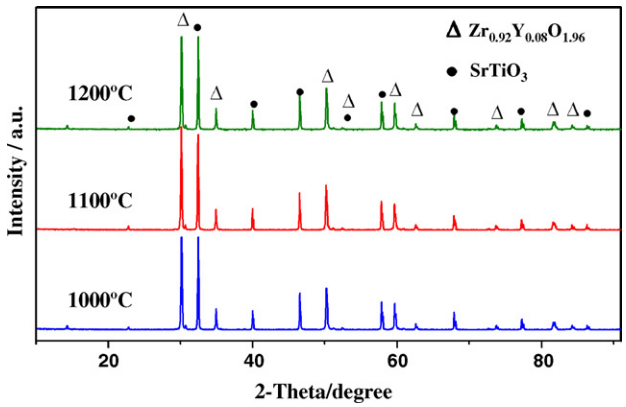

Fig. 9. XRD patterns for $Y_{0.08}Sr_{0.92}Ti_{0.99}O_{3-\delta}$/YSZ powder mixtures sintered at 1000, 1100 and 1200 °C for 10 h respectively in forming gas. No new impurity peaks were detected.

In order to assess the chemical compatibility of $Y_{0.08}Sr_{0.92}Ti_{1-x}O_{3-\delta}$ with YSZ electrolyte, powder mixture of $Y_{0.08}Sr_{0.92}Ti_{0.99}O_{3-\delta}$ and YSZ in the weight ratio of 1:1 was pressed into bars after milling for 6 h and then sintered at 1000, 1100 and 1200 °C for 10 h in forming gas, respectively. The sintered samples of $Y_{0.08}Sr_{0.92}Ti_{0.99}O_{3-\delta}$/YSZ were crushed to powders and examined by XRD, and the results are shown in Fig. 9. No impurity peaks were detected except for that assignable to $SrTiO_3$ and YSZ, indicating the good chemical compatibility of $Y_{0.08}Sr_{0.92}Ti_{0.99}O_{3-\delta}$ with YSZ below 1200 °C.

4. Conclusions

The limit of B-site deficiency in $Y_{0.08}Sr_{0.92}Ti_{1-x}O_{3-\delta}$ is below 5 mol % in forming gas at 1500 °C. Excessive deficiency in B-site will cause the formation of an insulating impurity (Y_2O_3). The B-site deficiency in $Y_{0.08}Sr_{0.92}Ti_{1-x}O_{3-\delta}$ results in the increase of oxygen ionic conductivity and the decrease of electronic conductivity. It is proposed that the deficiency of B-site elements in $Y_{0.08}Sr_{0.92}Ti_{1-x}O_{3-\delta}$ is charge compensated by the further formation of oxygen vacancies and the decrease of Ti^{3+} concentration. $Y_{0.08}Sr_{0.92}Ti_{1-x}O_{3-\delta}$ shows a relatively stable electrical conductivity at different oxygen partial pressures and exhibits an excellent chemical compatibility with YSZ electrolyte below 1200 °C. $Y_{0.08}Sr_{0.92}Ti_{1-x}O_{3-\delta}$ is a promising anode material for SOFCs.

Acknowledgements

This work was supported by National Nature Science Foundation of China (no. 50672009) and 863 Program of National High Technology Research Development Project of China (no. 2006AA11A189).

References

[1] J. Larminie, A. Dicks, Fuel Cell Systems Explained, 2nd ed., Cichester Wiley, 2003.
[2] E. Ivers-Tiffée, A.V. Virkar, in: S.C. Singhal, K. Kendall (Eds.), High-Temperature Solid Oxide Fuel Cells: Fundamentals, Design and Application, Elsevier Science, Oxford, 2003, p. 229.
[3] N.Q. Minh, J. Am. J. Eur. Ceram. Soc. 76 (1993) 563–588.
[4] S.C. Singhal, Solid State Ionics 135 (2000) 305–313.
[5] O. Yamamoto, Electrochim. Acta 45 (2000) 2423–2435.
[6] J.B. Goodenough, Y.H. Huang, J. Power Sources 173 (2007) 1–10.
[7] M.Y. Gonga, X.B. Liu, J. Power Sources 168 (2007) 289–298.
[8] J.P.P. Huijsmans, F.P.F. van Berkel, G.M. Christie, J. Power Sources 71 (1998) 107–110.
[9] M. Mogensen, K.V. Jensen, M.J. Jørgensen, S. Primdahl, Solid State Ionics 150 (2002) 123–129.
[10] F.H. Wang, R.S. Guo, Q.T. Wei, Y. Zhou, H.L. Li, S.L. Li, Mater. Lett. 58 (2004) 3079–3083.
[11] K. Hernadi, A. Fonseca, J.B. Nagy, A. Siska, I. Kiricsi, Appl. Catal. A199 (2000) 245–255.
[12] J.H. Koh, Y.-S. Yoo, J.-W. Park, H.C. Lim, Solid State Ionics 149 (2002) 157–166.
[13] A. Atkinson, S. Barnett, R.J. Gorte, J.T.S. Irvine, A.J. McEvoy, M. Mogensen, S.C. Singhal, J. Vohs, Nature 3 (1) (2004) 17–41.
[14] A. Atkinson, S. Barnett, J. Vohs, Nat. Mater. 3 (2004) 17.
[15] S.W. Tao, J.T.S. Irvine, Chem. Rec. 4 (2004) 83.
[16] O.N. Tufte, P.W. Chapman, Phys. Rev. 155 (1967) 796–802.
[17] H.P.R. Frederikse, W.R. Hosler, Phys. Rev. 161 (1967) 822–827.
[18] O.A. Marina, N.L. Canfield, J.W. Stevenson, Solid State Ionics 149 (2002) 21–28.
[19] X. Huang, H. Zhao, W. Shen, W. Qiu, W. Wu, J. Phys. Chem. Solids 67 (2006) 2609–2613.
[20] X. Li, H. Zhao, W. Shen, F. Gao, X. Huang, Y. Li, Z. Zhu, J. Power Sources 166 (2007) 47–52.
[21] S.Q. Hui, A. Petric, J. Eur. Ceram. Soc. 22 (2002) 1673–1681.
[22] X. Li, H. Zhao, F. Gao, Z. Zhu, N. Chen, W. Shen, Solid State Ionics 179 (2008) 1588–1592.